Cross-wake force and correlated head-tail instability in beam-beam collisions with a large crossing angle

Nami Kuroo,[1,3] Kazuhito Ohmi,[1,*] Katsunobu Oide,[1,2] Demin Zhou,[1,2] and Frank Zimmermann[2]

[1]*KEK, Tsukuba, Ibaraki 305-0801, Japan*
[2]*CERN, 1211 Geneva 23, Switzerland*
[3]*University of Tsukuba, Tsukuba, Ibaraki 305-8577, Japan*

(Received 5 January 2018; published 15 March 2018)

This paper discusses novel coherent beam-beam instability in collisions with a large crossing angle. The instability appears in the correlated head-tail motion of two colliding beams. A cross-wake force, which is localized at the collision point, is introduced to represent the head-tail correlation between colliding beams. A mode-coupling theory based on this localized cross-wake force enables us to explain the correlated heal-tail instability. The use of a collision scheme with a large crossing angle is becoming popular in the design of electron–positron colliders. An example thereof is the SuperKEKB project, in which a collision with a large crossing angle is performed to boost the luminosity to 0.8×10^{36} cm^{-2} s^{-1}. Future circular colliders will also be designed with a large crossing angle. Strong-strong simulations, which have shown the first coherent head-tail instability, can limit the performance of proposed future colliders. The mechanism whereby this instability occurs is mode coupling due to the cross-wake force. This instability may affect all collider designs based on the crab waist scheme.

DOI: 10.1103/PhysRevAccelBeams.21.031002

I. INTRODUCTION

An ordinary transverse wake force characterizes a transverse momentum kick of a particle at z according to the dipole moment density at z' in a bunch:

$$\Delta p_x(z) = -\int_z^\infty W(z-z')\rho_x(z')dz'. \tag{1}$$

Based on the causality, the head part of the dipole moment affects the tail part of the particles, $W(z-z') \neq 0$ for $z' > z$. p_x, which is normalized by the total momentum, is dimensionless. The dipole moment is expressed by $\rho_x(z) = x(z)\rho(z)$, which is the product of the dipole amplitude and normalized density distribution along z. $W(z)$, which is expressed by $Nr_eW(z)/\gamma$ in the conventional formula [1], contains the bunch population and γ factor.

In a beam-beam collision with a crossing angle, a transverse dipole moment $\rho_x^{(\pm)}(z')$ of an $e^\pm$ beam can induce a transverse momentum kick of a colliding $e^\mp$ beam. We consider the cross-wake force to represent the momentum kick as follows [2,3]:

$$\Delta p_x^{(\pm)}(z) = -\int_{-\infty}^\infty W_x^{(\pm)}(z-z')\rho_x^{(\mp)}(z')dz'. \tag{2}$$

The momentum kick is significant in the area $|z-z'| \sim \sigma_x/\theta_c$ where two beams overlap, where σ_x and θ_c are the horizontal beam size and half-crossing angle, respectively. The wake force is independent of the sign of $z-z'$, that is, there is no causal property, unlike the ordinary wake force. Another important point is that the cross-wake force is localized at the point at which the two beams interact, and this localized wake force is used as the basis on which the mode-coupling theory is developed. The theory explains that the wake force can cause coherent beam-beam instability, in which correlated head-tail modes between two beams are induced.

The "crab waist collision" scheme [4,5], which has become popular for circular e^+e^- colliders, forms the basis for the design of several future colliders. The crab waist collision is premised on the large crossing angle collision. The SuperKEKB accelerator adopts the collision scheme with a large crossing angle to boost the luminosity to 0.8×10^{36} cm^{-2} s^{-1}. Future circular colliders (FCCs) will also be designed based on the crab waist scheme with a large crossing angle [6–8]. However, strong-strong beam-beam simulations have shown instability in collisions with a large crossing angle [3,9–12]. The present mode-coupling theory for the cross-wake force explains the instability observed in the simulations. Understanding this instability is indispensable for future accelerator designs.

This paper is organized as follows. The cross-wake force is introduced in Sec. II. The wake force is regarded as a

*Corresponding author.
ohmi@post.kek.jp

conventional single-bunch wake force when the coherent beam-beam mode is limited to either the σ or π mode. Ordinary mode-coupling theory is applied to the single-bunch wake force. Particle-tracking simulations using the cross- and single-bunch wake forces are discussed in Sec. III. The simulations imply that the instability occurs only for a localized wake force. The mode-coupling theory for the localized single-bunch wake force is discussed in Sec. IV. The mode-coupling theory is extended for two beams for the cross-wake force in Sec. V. Section VI draws some conclusions.

II. CROSS-WAKE FORCE INDUCED BY BEAM-BEAM COLLISION

We begin by discussing cross-wake force induced by beam-beam collisions with a large crossing angle. Figure 1 illustrates the method by which to evaluate the cross-wake force. Two beams (bunches) collide with a half-crossing angle θ_c. The region in which the two bunches overlap at the collision point is $\Delta z = \pm\sigma_x/\theta_c$. Using the Lorentz transformation for the x-direction, the bunches e^-/e^+ with a tilt angle θ_c move to the left/right, respectively, at the speed of light [13,14]. Electromagnetic fields of the relativistic $e^\pm$ bunches are formed in the transverse plane. The parts in the $e^\pm$ bunches at the same s position interact with each other. We assume a Gaussian distribution of bunches in the transverse plane.

The momentum kick of the $e^\mp$ bunch at z, which collides with a part of the $e^\pm$ bunch with length $\delta z'$ at z', can be expressed by

$$\delta p_y^{(\mp)}(x,y) + i\delta p_x^{(\mp)}(x,y) = \frac{N^{(\pm)}\rho^{(\pm)}\delta z' r_e}{\gamma^{(\mp)}} F(x,y), \tag{3}$$

where (x,y) is the relative position vector between the transverse center of the bunches at z ($e^\mp$) and z' ($e^\pm$), and $N^{(\pm)}\rho^{(\pm)}(z')\delta z'$ is the number of particles contained in the $\delta z'$ of the $e^\pm$ bunch. Interaction between the bunches with z, z' occurs at $s = (z-z')/2$. F is represented by the complex error function w [15]:

$$F = F_y + iF_x = \frac{2\sqrt{\pi}}{\Sigma}[w(A) - \exp(-B)w(C)], \tag{4}$$

where A, B, C are defined as follows:

$$A = \frac{x+iy}{\Sigma}, \qquad B = \frac{x^2}{4\bar{\sigma}_x^2} + \frac{y^2}{4\bar{\sigma}_y^2}, \qquad C = \frac{\frac{\bar{\sigma}_y}{\bar{\sigma}_x}x + i\frac{\bar{\sigma}_x}{\bar{\sigma}_y}y}{\Sigma}, \tag{5}$$

where $\Sigma = 2\sqrt{(\bar{\sigma}_x^2 - \bar{\sigma}_y^2)}$. The root mean of the beam sizes is $\bar{\sigma}_{x,y}^2 = (\sigma_{x,y}^{(+)2} + \sigma_{x,y}^{(-)2})/2$.

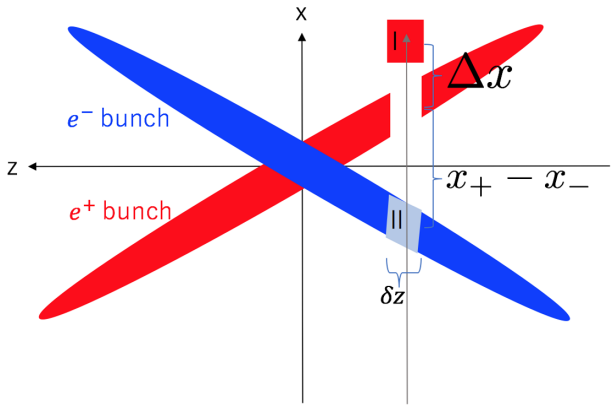

FIG. 1. Illustrative representation of the evaluation of the cross-wake force.

Part of the e^+ bunch "I" at z' deviates by Δx in the x-direction, as shown in Fig. 1. The part marked "II" at z of the e^- bunch interacts with the deviated part of the e^+ bunch.

The part II (z) colliding with I shifts as the collision progresses. The cross-wake force is given by the difference between momentum kicks with and without the deviation Δx. For a collision with a crossing angle, the horizontal offset is related to the longitudinal position of a bunch by $x = z\theta_c$. The difference in the momentum kick is expressed by

$$\begin{aligned}\Delta p_x^{(-)} &\equiv \delta p_x^{(-)}(x_- - x_+ - \Delta x) - \delta p_x^{(-)}(x_- - x_+) \\ &= \frac{N^{(+)}\rho^{(+)}(z')\delta z' r_e}{\gamma^{(-)}} \left.\frac{\partial F_x}{\partial x}\right|_{x=(z-z')\theta_c} \Delta x_+. \end{aligned} \tag{6}$$

The cross-wake force is determined by the right side of Eq. (6), expressed as follows:

$$\Delta p_x^{(-)} = -W^{(-)}(z-z')\rho^{(+)}\Delta x_+ \delta z. \tag{7}$$

Using $\rho(z')\Delta x = \rho_x(z')$, the cross-wake force is given by the differential of the beam-beam force as follows:

$$W_x^{(-)}(z-z') = -\frac{N^{(+)}r_e}{\gamma^{(-)}} \left.\frac{\partial F_x}{\partial x}\right|_{x=(z-z')\theta_c} \tag{8}$$

$\partial F/\partial x$ can be written as follows:

$$\begin{aligned}\frac{\partial F}{\partial x} = \frac{2\sqrt{\pi}}{\Sigma}\Bigg[&\frac{2i}{\sqrt{\pi}\Sigma}\left(1 - \frac{\sigma_y}{\sigma_x}\exp(-B)\right) \\ &- \frac{2A}{\Sigma}w(A) + \left\{\frac{x}{\sigma_x^2} + \frac{2\sigma_y}{\Sigma\sigma_x}C\right\}\exp(-B)w(C)\Bigg], \end{aligned} \tag{9}$$

where the differential formula of the complex error function, $w'(z) = -2zw(z) + 2i/\sqrt{\pi}$, is used.

We consider the reaction of the force for the positron beam in Eq. (7):

$$\Delta p_x^{(+)}(z') = -\frac{N^{(-)} r_e}{\gamma^{(+)}} \left.\frac{\partial F_x}{\partial x}\right|_{x=(z-z')\theta_c} \rho^{(-)}(z)\delta z \times \Delta x_+. \tag{10}$$

This force induces a tune shift, the term for which is added in Eq. (2):

$$\Delta p_x^{(\pm)}(z) = -\int_{-\infty}^{\infty} W_x^{(\pm)}(z-z')\rho_x^{(\mp)}(z')dz' + \int_{-\infty}^{\infty} W_x^{(\pm)}(z-z')\rho^{(\mp)}(z')dz' x^{(\pm)}(z). \tag{11}$$

The coefficient of $x^{(\pm)}(z)$ in the second term contains z. It is straightforward to treat Eq. (11) in particle-tracking simulations.

Integrating over z, this momentum kick gives the horizontal beam-beam tune shift for the positron beam [16,17]. We now assume collisions between two Gaussian bunches. Thus, the tune shift is half of the nominal value. The tune shift gives an offset of the horizontal tune in mode-coupling analysis. We basically study the first term, which is attributed to beam instabilities. The effects of the tune shift are discussed toward the end of Sec. IV.

In recent e^+e^- colliders, the aspect ratio of the beam size at the interaction point is very small; both the emittance coupling $\varepsilon_y/\varepsilon_x$ and beta ratio β_y^*/β_x^* are less than 1%, thus, $\sigma_y/\sigma_x < 0.01$. Neglecting the dependence on y and $\bar{\sigma}_y$, the wake force is expressed using $A = x/(2\bar{\sigma}_x)$, $B = A^2$, and $C = 0$ as follows:

$$W_x^{(-)}(z) = -\frac{N^{(+)} r_e}{\gamma^{(-)}\bar{\sigma}_x^2}\left[1 - \frac{\sqrt{\pi}\theta_P z}{2\bar{\sigma}_z}\mathrm{Im}w\left(\frac{\theta_P z}{2\bar{\sigma}_z}\right)\right], \tag{12}$$

where $\theta_P = \theta_c\bar{\sigma}_z/\bar{\sigma}_x$ is the Piwinski angle [18]. The normalized wake force is defined by

$$W_N(\zeta) = -1 + \sqrt{\pi}\zeta/2\mathrm{Im}w(\zeta/2) = -1 + \zeta e^{-\zeta^2/4}\int_0^{\zeta/2} e^{u^2}du, \tag{13}$$

where $\zeta = \theta_P z/\sigma_z$. The cross-wake force for $e^{\pm}$ beams can be expressed by

$$W_x^{(\pm)}(z) = \frac{N^{(\mp)} r_e}{\gamma^{(\pm)}\bar{\sigma}_x^2} W_N(\zeta). \tag{14}$$

Figure 2 shows the normalized cross-wake force. This wake force is significant in an area several times the size of $\bar{\sigma}_z/\theta_P = \bar{\sigma}_x/\theta_c$. The characteristics of the wake force can be summarized as follows: $W = 0$ at $z \approx \pm 1.8\bar{\sigma}_x/\theta_c \pm 1.8\bar{\sigma}_z/\theta_P$. The maximal value is $W(z) \approx 0.28|W_x(0)|$ at $z \approx \pm 3.0\bar{\sigma}_x/\theta_c = \pm 3.0\bar{\sigma}_z/\theta_P$. The peak frequency of the wake is estimated as $\omega = 2\pi c/\lambda = 2\pi c\theta_P/6.0\bar{\sigma}_z$, because of $\lambda = 6.0\bar{\sigma}_z/\theta_P$. The oscillation period of the frequency in a bunch is $\omega\bar{\sigma}_z/c \approx \theta_P$.

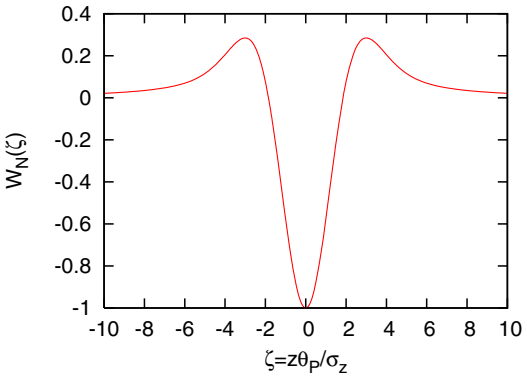

FIG. 2. Normalized cross wake force, $W_N(\zeta) = -1 + \sqrt{\pi}\zeta/2\mathrm{Im}w(\zeta/2)$, where $\zeta = \theta_P z/\sigma_z$.

The corresponding impedance is obtained by the Fourier transform of the wake force,

$$Z^{(\pm)}(\omega) = i\int_{-\infty}^{\infty} W^{(\pm)}(z)e^{-i\omega z/c}\frac{dz}{c}. \tag{15}$$

The normalized cross impedance can be defined by the Fourier transformation of the normalized wake force.

$$Z_N(\upsilon) = i\int_{-\infty}^{\infty} W_N(\zeta)e^{-i\upsilon\zeta}d\zeta \tag{16}$$

The variable of the impedance is $\upsilon = \omega\bar{\sigma}_z/(c\theta_P)$. The cross impedance is related to the normalized one as follows:

$$Z^{(\pm)}(\omega) = \frac{N^{(\mp)} r_e}{\gamma^{(\pm)}\bar{\sigma}_x^2}\frac{\bar{\sigma}_z}{c\theta_P}Z_N(\upsilon). \tag{17}$$

Figure 3 shows the normalized cross impedance. The cross-wake force is symmetric for the sign of z. Therefore, the real part of the sine transform is 0. Only the imaginary part of the cosine transform is significant. Because the wake force has its minimum at $z = 0$ (the maximum in the absolute), it is dampened within one period. Therefore, the imaginary part of the impedance is negative.

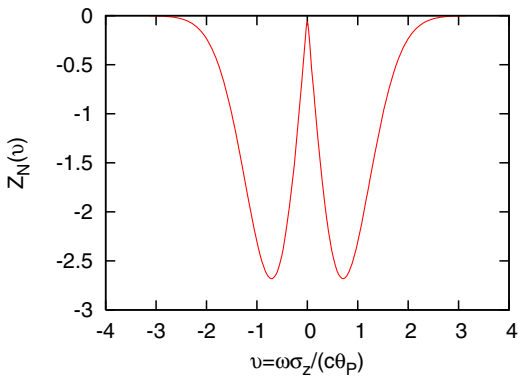

FIG. 3. Imaginary part of normalized cross impedance, where $\upsilon = \omega\bar{\sigma}_z/(c\theta_P)$.

We assume transparency conditions in which two beams have the same parameters in terms of their energy, bunch population, emittances, β^*, and tunes. By limiting the relation for the dipole moment distributions of the electron and positron bunches, the cross-wake force can be treated as a normal wake for a single bunch. The first mode is the σ mode, in which the dipole moment distributions of the two beams as a function of z are identical, $\rho_x^{(+)}(z) = \rho_x^{(-)}(z)$. The other is the π mode, in which the dipole moments are opposite, $\rho_x^{(+)}(z) = -\rho_x^{(-)}(z)$. Substituting the relation for $\rho_x^{(\pm)}$ into Eq. (2), the momentum kick can be expressed by the usual formula for a normal wake force,

$$\Delta p_x(z) = \mp \int_{-\infty}^{\infty} W_x(z - z')\rho_x(z')dz. \tag{18}$$

The equation represents an effective momentum kick given by a dipole moment distribution inside a bunch. Choosing the sign of the wake force, the behavior of the σ/π mode can be studied as exhibiting transverse single-bunch instability.

At the end of this section, we discuss the ordinary instability theory [1] for the wake force in Eq. (14). The beam distribution function for the dipole mode is expanded by the azimuthal and radial modes in longitudinal phase space. The tune for each mode is given by solving the matrix relation,

$$(\mu - \mu_x - l\mu_z)a_{kl} = \sum_{k'l'=-\infty}^{\infty} M_{kl,k'l'}a_{k'l'}, \tag{19}$$

where a_{kl} is the amplitude of the kth radial and lth azimuthal mode. Further, $\mu_x = 2\pi\nu_x$ and $\mu_z = 2\pi\nu_z$ are the betatron and synchrotron tunes, respectively. The tune $\mu = 2\pi\nu$ is obtained as an eigenvalue of the matrix, $(\mu_x + l\mu_z)\delta_{ll'}\delta_{kk'} + M_{kl,k'l'}$. The matrix is truncated for $0 \le k \le n_k - 1$ and $-l_{\max} \le l \le l_{\max}$, where n_k and $l_{\max}$ are integer numbers. Choosing of numbers is performed depending on the dominant modes caused by the wake force. In this regard, the convergence of the solution for n_k, $l_{\max}$ should be investigated. The matrix M is expressed by

$$M_{k\ell,k'\ell'} = \pm\frac{\beta_x}{2} i^{l-l'-1} \int_{-\infty}^{\infty} d\omega Z(\omega) g_{kl}(\omega) g_{k'l'}(\omega), \tag{20}$$

where

$$g_{kl}(\omega) = \frac{1}{\sqrt{2\pi k!(|l| + k)!}} \left(\frac{\omega\sigma}{\sqrt{2}c}\right)^{|l|+2k} e^{-\omega^2\sigma^2/2c^2}. \tag{21}$$

When the wake force has zero strength, the eigentune is $\mu_x + l\mu_z$. In the lowest perturbation, the diagonal components of M cause the modes to undergo tune shifts, which are expressed for the σ/π mode by

$$\Delta\nu_{kl} = \mp\frac{\beta_x}{2\pi} i Z_{kl,\mathrm{eff}} \tag{22}$$

where

$$Z_{kl,\mathrm{eff}} = \int_{-\infty}^{\infty} d\omega Z(\omega) g_{kl}(\omega) g_{kl}(\omega). \tag{23}$$

Here, $Z_{kl,\mathrm{eff}}$ is referred to as the effective impedance, which is purely imaginary and results in a pure real tune shift. The imaginary part of $Z_{kl,\mathrm{eff}}$ is negative; therefore, the tune shift is negative for the σ mode and positive for the π mode.

Considering the off-diagonal elements of M, Eq. (19) is solved as the eigenvalue problem. The matrix elements are given as the integration of the impedance with the bunch spectrum. The matrix elements are 0 for l, l' with different parities as the impedance is symmetric for the frequency. The matrix elements are retained for the exchange of $l \leftrightarrow l'$ and $k \leftrightarrow k'$ for l, l' with the same parity. That is, the matrix is real symmetric. As the eigenvalues of a real symmetric matrix are real, the wake force of Eq. (14) causes a tune shift, but this is not attributed to instability.

Equation (19) is given by an equation of motion, in which the wake force is applied continuously [1]. This wake force, which is induced by beam-beam interaction, is localized at the interaction point. The localized property is not considered in Eq. (19).

The normalized expression for M in Eq. (20) is obtained using the normalized expression of the impedance in Eq. (16):

$$M_{klk'l'} = \pi\xi_x(1 + \theta_P^2) i^{l-l'-1} N_{klk'l'}(\theta_P), \tag{24}$$

where ξ_x is the horizontal beam-beam tune shift:

$$\xi_x = \frac{N^{(\mp)} r_e}{2\pi\gamma\varepsilon_x^{\mp}} \frac{1}{1 + \theta_P^2}.$$

The normalized matrix $N_{klk'l'}$ is given as a function that only depends on θ_P:

$$N_{klk'l'}(\theta_P) = \int d\upsilon Z_N(\upsilon)\bar{g}_{kl}(\theta_P\upsilon)\bar{g}_{k'l'}(\theta_P\upsilon), \tag{25}$$

where

$$\bar{g}_{kl}(\theta_P\upsilon) = \frac{1}{\sqrt{2\pi k!(|l| + k)!}} \left(\frac{\theta_P\upsilon}{\sqrt{2}}\right)^{|l|+2k} e^{-\theta_P^2\upsilon^2/2}.$$

The matrix M, which appears again in the discussion concerning the localized wake force in Sec. IV, characterizes the beam instability phenomenon due to the cross-wake force. The matrix can be written using two parameters, the horizontal beam-beam tune shift and the Piwinski angle θ_P.

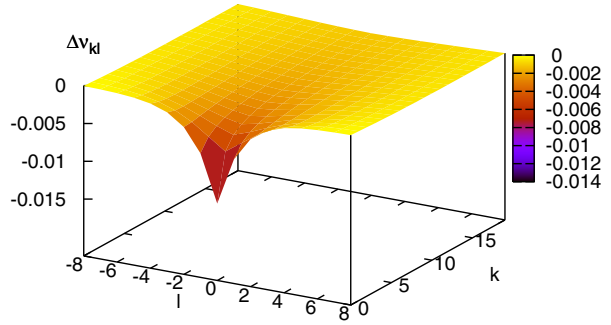

FIG. 4. Linear tune shift of the kl mode for the σ mode.

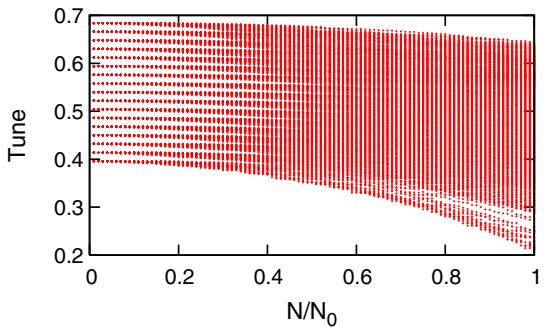

FIG. 5. Eigentune for $l_{\max} = 8, n_k = 20$.

Numerical examples are presented for the linear tune shift in Eq. (22) and eigenvalues (tune) for solving Eq. (19). The parameters are those that were employed for the high-luminosity version of FCCee-Z in 2016 [3,19], where the horizontal beam-beam tune shift and Piwinski angle are $\xi_x = 0.025$ and $\theta_P = 10$, respectively. Figure 4 shows the tune shift of each mode for the σ mode, which linearly depends on the bunch population for which the tune shift is real and negative. The largest tune shift has a negative value, $\Delta\nu = -\xi_x/2$, for $k = l = 0$. By contrast, the tune shift for the π mode, which is opposite to that of the σ mode, is positive.

The tune and instability growth are obtained by the eigenvalues solved by Eq. (19), which implies that no instability remains, because M is real symmetric. The bunch population is scanned from 0 to the design number $N_0 = 10^{11}$, where the tune shift is $\xi_x(N_0) = 0.025$. The eigentunes for every bunch population are calculated and plotted in Fig. 5, where the mode numbers are truncated at $l_{\max} = 8, n_k = 20$. The tunes, which are $\nu_x \pm l\nu_z$ for a zero-bunch population, shift linearly for a small population and then deviate from the linear slope for a larger population. Although the tunes overlap, imaginary parts do not appear.

III. PARTICLE TRACKING USING THE CROSS-WAKE FORCE

A. Tracking algorithm

We performed a particle-tracking simulation for the cross-wake force. The main purpose of the tracking simulation was to investigate the characteristics of the instability caused by the cross-wake force and obtain the keys to complete the theory. The beam particles experience beam-beam interaction, which is expressed by the cross-wake force, at the collision point. The beam traverses an arc section after/before the beam-beam interaction. In simulations, it is straightforward to represent the wake force localized at the collision point. The representation can be achieved by alternately performing transformations for the synchro-betatron motion in the arc section and for the cross-wake force at the interaction point.

The betatron and synchrotron variables (x, p_x, z, p_z) are transferred in the arc section by the following matrix:

$$M_i = \begin{pmatrix} \cos\mu_i & \beta_i \sin\mu_i \\ -\sin\mu_i/\beta_i & \cos\mu_i \end{pmatrix} \qquad i = x, z. \quad (26)$$

where the longitudinal beta is $\beta_z = -\sigma_z/\sigma_\delta$ and β_z is negative for positive momentum compaction.

The momentum kick due to the cross-wake force is expressed by Eq. (2). Here, Δp_x as a function of z depends on the longitudinal distribution of the dipole moment of the colliding beam.

The number of macroparticles generated by the Gaussian distribution with the beam size and bunch length in the transverse and longitudinal phase space is $N_{mp} = 10\,000$.

We take $\pm 3\sigma_z$ as the integration region for z'. The region is discretized by z_j with the width of $\Delta z = 0.02\sigma_z$. The density at z_j $[\rho(z_j)]$ is calculated by counting the number of particles (n_j) including $z_j \pm \Delta z/2$, $\rho(z_j) = n(z_j)/N_{mp}$. The dipole moment density $[\rho_x(z_j)]$ is the product of the average position and density $(\sum x_i/n(z_j) \times \rho(z_j) = \sum x_i/N_{mp})$ at z_j. The integral of Eq. (2) can be represented as follows:

$$\Delta p_x^{(\pm)}(z_j) = -\sum_{j'} W_x^{(\pm)}(z_j - z_{j'})\rho_x^{(\mp)}(z_{j'})\Delta z. \quad (27)$$

The momentum kick $[\Delta p_x(z)]$ at z is calculated by interpolating $\Delta p_x(z_j)$.

The simulation was performed to repeat the transformations in Eqs. (26) and (27). The variables for the macroparticles, $\langle x\rangle$, $\langle xz\rangle$, σ_x, and so on, were averaged in succession.

B. Simulation results

We first study the cases satisfying the transparency conditions. The head-tail instability caused by the cross-wake force was studied. $\langle xz\rangle/(\sigma_z\sigma_x)$, which is the dipole position $x(z)/\sigma_x$ at $z = \sigma_z$, informs the tilt of the beam for a simple head-tail motion with $l = 1$. Figure 6 presents the simulation result for SuperKEKB beta detuned eight times in both x and y [3,20,21], where the transparency condition for the $e^\pm$ beams is assumed to be satisfied such

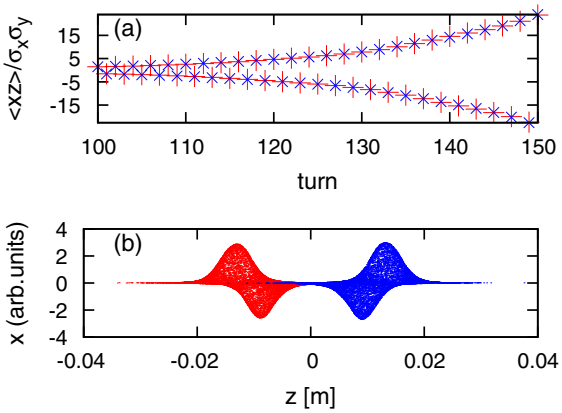

FIG. 6. Particle-tracking simulation of the two beams correlated by the cross-wake force in SuperKEKB with a detuned beta, $\xi_x = 0.0054$, $\theta_P = 8.0$ (transparent). (a) Evolution of $\langle xz \rangle$, and (b) beam distribution of the $x - z$ plane at the collision. The red and blue points represent the e^+ and e^- beams, respectively.

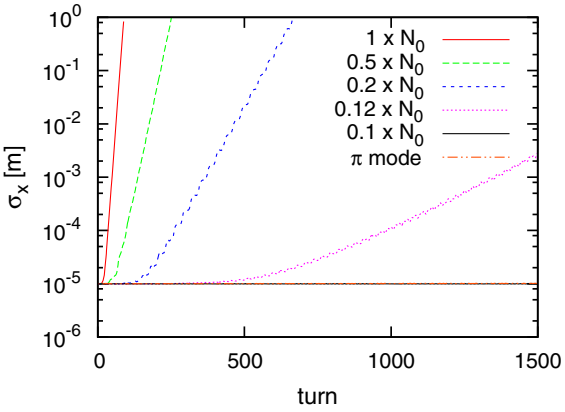

FIG. 7. Evolution of beam size for the single beam tracking simulation in FCCee-Z. Assuming the σ mode, ξ_x is scanned $\xi_x = 0.0025(N^{(\pm)} = 10^{10}) - 0.025(10^{11})$ in $\theta_P = 10$, $\nu_x = 0.54$, and $\nu_z = 0.018$. The last line is given for the π mode at $\xi_x = 0.025$.

that $\xi_x = 0.0054$ and $\theta_P = 8.0$. Plot (a) shows the evolution of $\langle xz \rangle / \sigma_z \sigma_x$ turn-by-turn. The evolution of the e^- and e^+ beams has the same value and their signs change alternately turn-by-turn. The phases of the oscillations are identical and the tune is 0.5. The growth time is approximately 30 turns.

Plot (b) presents the distributions of the e^-/e^+ bunch at the end of the tracking (300-th turn). The amplitude x is plotted in arbitrary units because the momentum kick is linear for x. The distributions of the two beams are identical, $\rho_x^{(+)}(z) = \rho_x^{(-)}(z)$, that is, the σ mode is induced. The distributions imply that the $l = \pm 1$ mode is dominant.

Systematic studies were performed using the parameters of FCCee-Z (HiLumi) [3], i.e., $\xi_x = 0.025$, $\theta_P = 10$, $\nu_x = 0.54$, and $\nu_z = 0.018$. The particle-tracking simulation for the single beam using Eq. (18) was performed assuming the σ mode. The bunch population was scanned in the range of $\xi_x = 0.0025$–0.025, corresponding to the bunch population of $N^{(\pm)} = 0.1$–$1.0 N_0$, in order to determine the threshold of the instability, where $N_0 = 1 \times 10^{11}$ is the design bunch population. Figure 7 shows the evolution of the horizontal beam size, where the design size is 10^{-5} m. The growth in the beam size appears at the threshold of the bunch intensity, $N^{(\pm)} = 0.12 N_0$, $\xi_x = 0.0030$. These simulations are based on linear theory. Thus, the beam size is not saturated. For the π mode, in which the plus sign of Eq. (18) is taken, the beam is stable at $\xi_x = 0.025$, $N^{(\pm)} = N_0$.

These results are in good agreement with the fact that the two-beam simulation for SuperKEKB exhibits only clear σ mode instability. The results for the two-beam simulation using the cross-wake force in FCCee-Z also provided the same result as in Fig. 7, and only the σ mode was observed.

In the previous section, we showed that the wake force did not cause instability in the ordinary theory. Equation (19) was derived for a continuously distributed wake force, whereas a head-tail instability appeared in the tracking simulation using a localized wake force.

This discrepancy in the appearance of instability is now discussed. The essential question is whether the wake force is localized at the interaction point or uniformly distributed in the ring. We investigated this by comparing the cases in the tracking simulation in which the wake force is localized and distributed. The distributed wake force was simulated by dividing both the strength of the wake and the synchrotron phase advance into $n_{\rm div} = 1, 2, 5, 8, 10$. The particles experience a reduced wake force $n_{\rm div}$ times in a revolution. Figure 8 shows the evolution of the horizontal beam size for $n_{\rm div}$. The instability appears when the number of divisions reaches $n_{\rm div} \leqq 8$. This indicates that the instability is only caused by the "localized" cross-wake force.

We next investigated the dependency of the unstable mode on the horizontal tune. Figure 9 presents the $x - z$

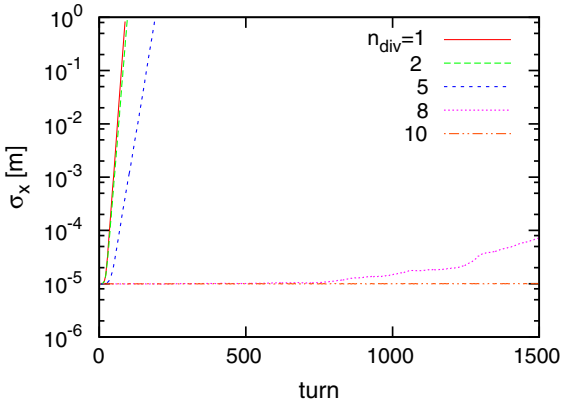

FIG. 8. Evolution of beam size for single beam tracking in FCCee-Z. The bunch population (ξ_x) and synchrotron tune are divided into $n_{\rm div} = 1, 2, 5, 8, 10$ in a revolution.

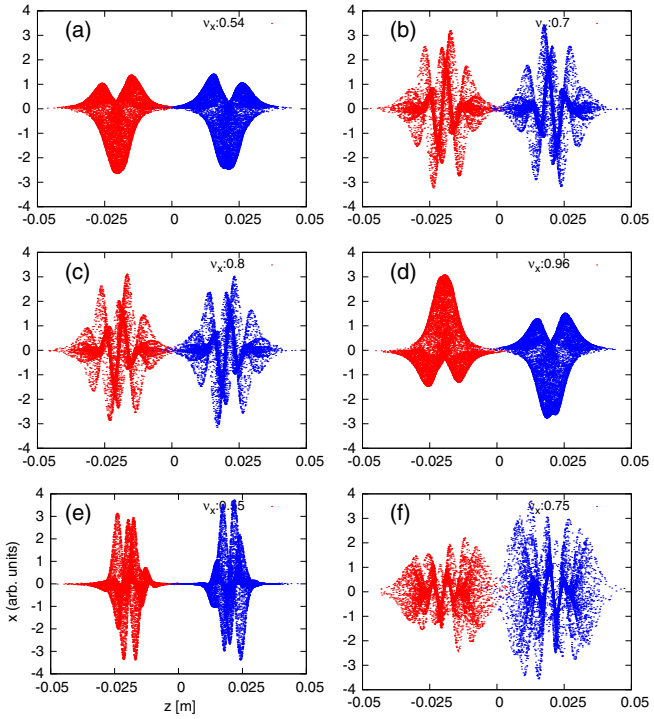

FIG. 9. Beam distribution in the $x-z$ plane at the collision point in FCCee-Z. The horizontal tunes are (a) $\nu_x = 0.54$, (b) $\nu_x = 0.7$, (c) $\nu_x = 0.8$, (d) $\nu_x = 0.96$, (e) $\nu_x = 0.55$, $N = 0.4N_0$, and (f) $\nu_x = 0.75$.

distribution in the instability for various parameters of FCCee-Z. Plots (a), (b), (c), and (d) present the distributions for $\nu_x = 0.54$, 0.7, 0.8, and 0.96, respectively. The instability occurs in the σ mode at the design tune $\nu_x = 0.54$. The azimuthal mode appears to be $l = \pm 2$. Plots (a) and (d) have very similar distributions, except for the difference between the σ and π modes. Plots (b) and (c) have complex distributions; thus, a high-order azimuthal mode seems to be induced. The latter two plots are also very similar, except for the σ and π modes, i.e., π mode instability is dominant in the horizontal tune $\nu_x > 0.75$.

These results indicate that the beam-beam modes were clearly separated. That is, either the σ or π mode was observed. We can conclude that the wake force model assuming either the σ or π mode in Eq. (18) is plausible. Furthermore, whether the σ or π mode appears depends on the horizontal tune: the σ mode appears for $0.5 < \nu_x < 0.75$, whereas the π mode appears for $0.75 < \nu_x < 1$. The unstable eigenmodes are almost identical for the symmetric point of $\nu_x = 0.75$, except for σ or π.

The π mode instability can be observed depending on the parameters even if the tune is $\nu_x < 0.75$. An example is shown in plot (e), where the bunch intensity is lower and shows that $\xi_x = 0.01$, $0.4N_0$, and $\nu_x = 0.55$.

An interesting case is for $\nu_x = 0.75$. Plot (f) presents the $x-z$ distribution of the unstable mode for N_0. Instability with a complex mode structure can be seen.

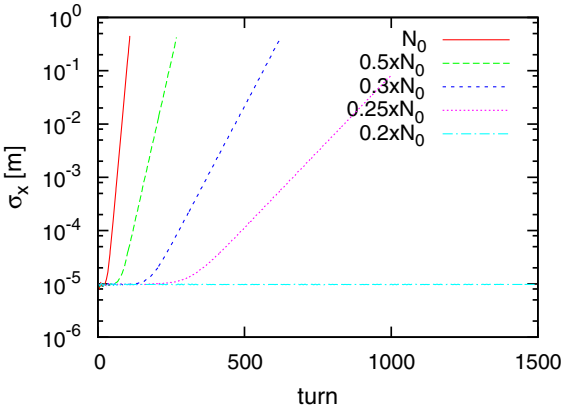

FIG. 10. Evolution of the beam size for the single beam tracking simulation including the tune shift using Eq. (11) in FCCee-Z, where $\theta_P = 10$, $\nu_x = 0.54$, $\nu_z = 0.018$ and $\xi_x = 0.025$ at N_0.

Here, we take into account the tune shift depending on z in Eq. (11). Figure 10 shows the evolution of the horizontal beam size. The threshold of the bunch intensity is $N^{(\pm)} = 0.25N_0$, $\xi_x = 0.006$. The distribution of the two beams is almost the same as in Fig. 7(a). That is, the azimuthal mode is $l = \pm 2$.

Thus far, we have studied cases satisfying the transparency conditions. For asymmetric colliders such as SuperKEKB, the parameters are different for the $e^{\pm}$ beams. The horizontal beam-beam tune shifts are $\xi_x^{(+)} = 0.0174$ and $\xi_x^{(-)} = 0.0099$ for the e^+ and e^- beams, respectively, in the operation with the detuned beta ($8 \times \beta_{xy}, \theta_P = 8$). The synchrotron tunes are $\nu_z^{(+)} = 0.0244$ and $\nu_z^{(-)} = 0.028$. When both horizontal tunes are the same for the design number $\nu_x = 0.53$, the induced mode closely approximates the σ mode. We show a special example for the tunes $\nu_x^{(-)} = 0.57$ and $\nu_x^{(+)} = 0.53$ in which neither the σ nor the π mode

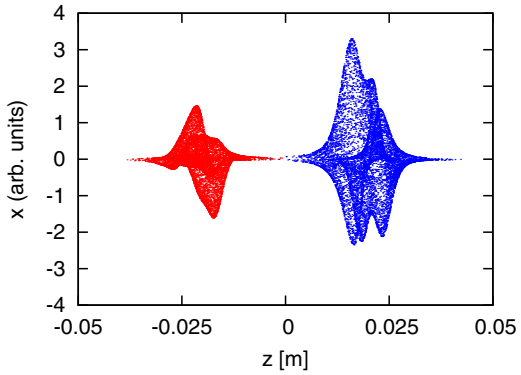

FIG. 11. Beam distribution in the $x-z$ plane at the collision point for $\nu_x^{(-)} = 0.57$ and $\nu_x^{(+)} = 0.53$ (SuperKEKB), where $\theta_P = 8$, $\xi_x^{(+)} = 0.0174$, $\xi_x^{(-)} = 0.0099$, $\nu_z^{(+)} = 0.0244$, and $\nu_z^{(-)} = 0.028$.

can be an eigenmode. Figure 11 presents the $x-z$ distributions of the two beams. The structure of the e^- beam is more complex than that of the e^+ beam. The number of azimuthal (l) modes of the e^- beam appears to be larger than those of the e^+ beam.

IV. EIGENVALUE PROBLEM FOR LOCALIZED SINGLE-BEAM WAKE FORCE

A. Formalism for localized single-beam wake force

We develop a mode-coupling theory guided by the results of the tracking simulations in the previous section. The wake force we are studying here is localized at the interaction point as it is induced by the beam-beam interaction. In Sec. II, we considered a wake force that was uniformly distributed in a ring using Eq. (19). The localized property of the wake force was not considered, Thus, the instability was not caused by the wake force. The localized property in the tracking simulation was considered by alternately performing transformations for the synchro-betatron motion and wake force. Instability was only observed for the particle tracking using the localized wake force. We develop a mode-coupling theory based on the same algorithm by alternately performing transformations. A similar study for a localized wake force is reported in Ref. [22].

Let $\Psi(x,p_x,z,\delta;t)$ be the distribution function of the phase space at the collision point, where t is the time in units of revolution time. x, p_x are normalized by $p\sqrt{\beta_x}\to p$ and $x/\sqrt{\beta_x}\to x$. The density in longitudinal space is given by

$$\psi(J)=\int \Psi dx dp_x \qquad \rho(z)=\int \psi(z,\delta)d\delta. \tag{28}$$

The density is assumed to be Gaussian in longitudinal phase space $\psi(J)=\exp(-J/\varepsilon_z)/(2\pi\varepsilon_z)$, as a function only of $J=(z^2/\beta_z+\beta_z\delta^2)/2$, where ψ and ρ are independent of t. The horizontal amplitude in longitudinal phase space and dipole moment distribution in z are expressed by

$$x(J,\phi;t)=\frac{\int x\Psi dx dp_x}{\psi(J)}$$
$$\rho_x(z;t)=\int x(J,\phi;t)\psi(J)d\delta. \tag{29}$$

$p_x(J,\phi;t)$ is given by a similar formula in which x is replaced with p_x.

$[x(J,\phi;t),p_x(J,\phi;t)]$ is transferred to $[x(J,\phi;t+1),p_x(J,\phi;t+1)]$ by the matrix for the betatron motion in the arc section as follows:

$$M_\beta=\begin{pmatrix}\cos\mu_x & \sin\mu_x\\ -\sin\mu_x & \cos\mu_x\end{pmatrix}, \tag{30}$$

For the synchrotron motion, the position of the longitudinal phase space (J,ϕ) is transferred to $(J,\phi+\mu_s)$,

$$x(J,\phi+\mu_s;t+1)=x(J,\phi;t). \tag{31}$$

The momentum change due to the wake force can be expressed using Eq. (29) as follows:

$$\Delta p_x(J,\phi;t)=\mp\int W_x(z-z')x(J',\phi';t)\psi(J')dJ'd\phi'. \tag{32}$$

Equations (30), (31), and (32) are the linear transformations for $[x(J,\phi;t),p_x(J,\phi;t)]$. The combined transformation multiplied by these three represents one revolution, t to $t+1$. The transformations, which are the synchro-betatron motion and the wake force at the interaction point, are performed alternately. The localized property of the wake force is now considered. The transformation is independent of t.

When the revolution transformation is expressed by a matrix with a size that is approximately finite, the stability of the colliding system can be studied by the eigenvalues/vectors of the revolution matrix.

One method to obtain a matrix with finite size is to discretize the longitudinal phase space, J_i, ϕ_j [23]. The dipole amplitudes can be expressed by

$$x_{ij}=x(J_i,\phi_j;t) \qquad p_{ij}=p_x(J_i,\phi_j;t). \tag{33}$$

The synchrotron tune is assumed to be the inverse of an integer $n_z=1/\nu_z$; ϕ is $\phi_j=2\pi j\nu_z$. J_i is divided as $\sqrt{J_i}=i\Delta_J\sqrt{\varepsilon_z}$, $i=1,n_J$. n_J, Δ_J are chosen such that the dominant head-tail modes are sufficiently represented. The convergence of n_J should be investigated. The size of the matrix is $2\times n_J\times n_z$. The synchrotron motion of Eq. (31) is represented by the transformation of j to $j+1$. Matrix M_0 for the transformation of the synchro-betatron motion is given by [3]

$$M_0=\delta_{i,i'}\delta_{j-1,j'}\begin{pmatrix}\cos\mu_x & \sin\mu_x\\ -\sin\mu_x & \cos\mu_x\end{pmatrix}. \tag{34}$$

The transformation for the momentum kick due to the wake force M_W can be expressed by

$$M_W=\begin{pmatrix}\delta_{i.i'}\delta_{j,j'} & 0\\ -\beta_x W(z_{i,j}-z_{i',j'})\psi_{i'}\Delta J\Delta\phi & \delta_{i.i'}\delta_{j,j'}\end{pmatrix}. \tag{35}$$

The matrices M_W, M_0, and the revolution matrix of their product are symplectic. The eigenvalues of the revolution matrix appear as pairs of $\lambda=e^{\pm i\mu}$. When μ is complex, their complex conjugates $\lambda^*=e^{\mp i\mu^*}$ are also eigenvalues. We refer to $\nu=\mu/2\pi=\nu_R+i\nu_I$ as an eigentune. The real part $\pm\nu_R$ is ambiguous for an integer. There are three cases of eigenvalues of the symplectic matrix [24]: (1) A pair of eigenvalues represented by $e^{\pm i\mu}$ for a real μ. The real part of

the tune is $\pm\nu_R$. The tune can fall within the range of 0–0.5 or 0.5–1. The modes corresponding to the eigenvalues are stable. (2) A pair of eigenvalues represented by $e^{\pm\mu_I}$ or $-e^{\pm\mu_I}$ for the purely imaginary $\mu = i\mu_I$. The real part of the eigentune is 0 or 0.5 depending on the sign of the eigenvalue. This is known as an integer or half-integer resonance. The two modes with the eigenvalues $e^{\pm\mu_I}$ are the growth and damping modes with the same rate. (3) A set of eigenvalues consists of four values, $e^{\pm i\mu}$ and $e^{\mp i\mu^*}$ for a complex $\mu = \mu_R + i\mu_I$. The four modes with the eigenvalues $e^{\pm i\mu_R \pm \mu_I}$, which have two tunes $\pm\nu_R$, are the growth and damping modes with the same rate. The tune can occur within the range of 0–0.5 or 0.5–1.0. The four eigenvalues basically originate from two modes. The coupling between the two modes results in modes represented by a complex value containing imaginary μ. This is known as mode coupling. The colliding beams are stable when all μ values are real, whereas they are unstable when one or more μ values are complex.

An eigenvector corresponding to an eigenvalue provides the mode for $[x(J,\phi), p_x(J,\phi)]$ with the eigentune. The growth rate per revolution and the real part of the tune are given by taking the eigenvalues as $\log|\lambda|$ and $\tan^{-1}(\mathrm{Im}\lambda/\mathrm{Re}\lambda)/(2\pi)$, respectively. The eigenvalues are plotted in Fig. 5 of Ref. [3]. Here, we present the eigenvector with the fastest growth rate in Fig. 12. The (J,ϕ) space is discretized by $\Delta_J = 0.05, n_J = 40$. The circular area of the (J,ϕ), (z,δ) space is $\sqrt{2J_{\max}/\varepsilon_z} = z_{\max}/\sigma_z = \delta_{\max}/\sigma_\delta = 2\sqrt{2}$. The surface on the (z,δ) space represents the dipole amplitude distribution of the most unstable mode. There are two peaks along the azimuth angle, such that the number of modes is $l = \pm 2$.

We next consider the dipole modes expanded by azimuthal and radial modes as achieved in Eqs. (19) and (20) [1],

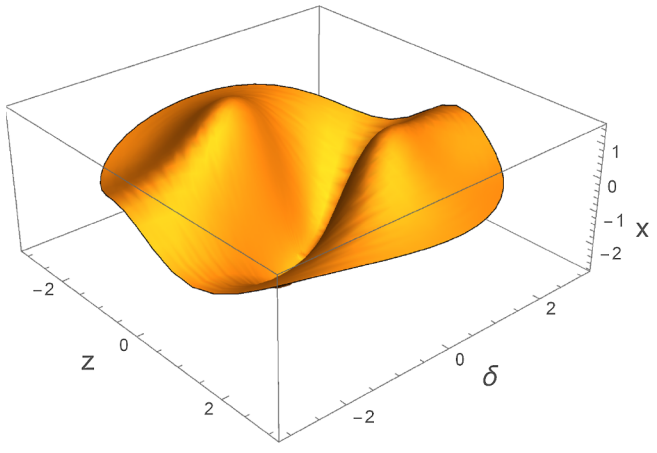

FIG. 12. Eigenvector of an unstable mode with the fastest growth rate. The z and δ axes are in units of σ_z and σ_δ, respectively. x is in arbitrary units.

$$x(J,\phi;t) = \sum_{l,k} x_{kl}(t)\sqrt{\frac{k!}{(|l|+k)!}}\hat{J}^{|l|/2}L_k^{(|l|)}(\hat{J})e^{il\phi}, \tag{36}$$

where $L_k^{(l)}$ is the Laguerre polynomial. $p_x(J,\phi;t)$ is expanded in the same manner. The summation of l and k is terminated by $\pm l_{\max}$ and $k_{\max} = n_k - 1$, respectively. The length of the dipole moment vector (x_{kl}, p_{kl}) is $2(2l_{\max}+1)n_k$.

The vector is transferred for $t \to t+1$ by the matrix M_0 for synchro-betatron motion in the arc section as follows:

$$M_0 = e^{-2\pi i l\nu_z}\delta_{kk'}\delta_{ll'}\begin{pmatrix} \cos\mu_x & \sin\mu_x \\ -\sin\mu_x & \cos\mu_x \end{pmatrix}. \tag{37}$$

The momentum change for modes due to the wake force can be expressed by

$$\Delta p_{kl}(t) = -2\sum_{k'l'} M_{klk'l'}x_{k'l'}(t). \tag{38}$$

The matrix $M_{klk'l'}$, which is given in Eq. (20), is a real and symmetric matrix and has off-diagonal elements between modes with the same parity for l and l'. The vector (x_{kl}, p_{kl}) is transferred by the wake force as follows:

$$M_W = \begin{pmatrix} 1 & 0 \\ -2M_{klk'l'} & 1. \end{pmatrix} \tag{39}$$

The stability can be discussed by solving the eigenvalue problem for the revolution matrix, $M_W M_0$. Incidentally, the tune shift formula, $\Delta\nu = K\beta_x/4\pi$, $K = 2M_{klk'l'}$, gives Eq. (19).

The matrices M_W, M_0, and their product are symplectic. The three cases mentioned above apply here as well. The real part of the eigentune appears at $\nu_R \sim \nu_x \pm l_{\max}\nu_z$. The tune can either occur within the range of 0–0.5 or 0.5–1.0. The tune is wrapped when it crosses a half-integer or integer. Both modes with $\pm\nu_R$ experience growth and damping at the same rate.

B. Eigensystem for single-beam wake force

Here, the eigenvalue problem for a single beam is solved for FCC-ee-Z, $\xi_x = 0.025$, $\theta_c = 10$. We first discuss the results for the design tune, $\nu_x = 0.54$, $\nu_z = 0.018$. Figure 13 shows the growth rate for the σ/π modes, where $l_{\max} = 8, k_{\max} = 20$ are chosen. The tune is terminated at $0.54 + 0.018 \times 8 = 0.684$. For negative values of l, it is wrapped and terminated at $1 - (0.54 - 0.018 \times 8) = 0.604$.

The σ modes are unstable, whereas all the π modes are stable. The unstable tunes are terminated at $0.5 + m\nu_z \approx 0.6$, $m \le 7$, because of $l_{\max} = 8$. The equivalent value was $m \le 14$ for the first method using Eqs. (34) and (35) in Fig. 5 of Ref. [3]. The most unstable mode is at $\nu = 0.5$

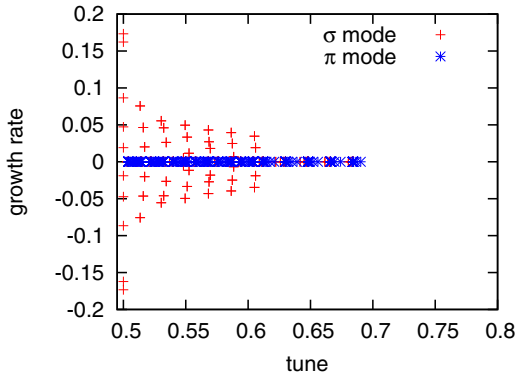

FIG. 13. Growth rate for each eigenmode as a function of the eigenmode tune for a bare tune $\nu_x = 0.54$ in FCCee-Z. The red and blue points in the plot represent the σ and π modes, respectively.

and the growth rate is 0.18/turn. Thus, the result is consistent with the previous result [3] for the dominant modes. This result confirms that the assumption $\nu_z = 1/n_z$ and the choice of $l_{\max}, k_{\max}$ in this method are reasonable.

Plotting the eigentune spectrum as a function of the bunch population is helpful for illustrating the mode-coupling feature. The bunch population is used as a control parameter for the wake force strength. The eigenvalues are calculated and plotted for scanning the bunch population $N^{(\pm)} = 0 - N_0$, where $N_0 = 1 \times 10^{11}$ in FCCee-Z. Figure 14 presents the eigenvalues as a function of the bunch population. Plots (a) and (b) show the tune (ν_R) and growth rate (μ_I) for the σ (red points) and π (blue) modes, respectively. In the plots, the lines start from $\nu = \nu_x + l\nu_z$ at $N = 0$, $\nu = 0.504, 0.522, 0.54, 0.558, 0.576, \ldots$, which are synchrotron sidebands. For $\nu < 0.5$, ν, which is wrapped, the results are $\nu = 1 - (\nu_x + l\nu_z)$ for $l \leq -3$. For $l = -3, -4, -5$, ν is 0.514, 0.532, and 0.55, respectively, at $N^{(\pm)} = 0$.

The σ mode is plotted using red points. The tune shift is negative for the σ mode in this model. An instability appears when the $l = -2, \nu = 0.504$ mode approaches 0.5 at $N^{(\pm)} \approx 0.1N_0$. A half-integer resonance arises for the $l = -2$ mode. At similar $N^{(\pm)} \approx 0.1N_0$, the $l = -1, -3$ and $l = 0, -4$ modes merge and an imaginary tune appears. Mode coupling occurs between modes with the same parity. Increasing the wake strength, modes $l = 1, -5$, $l = 2, -6$, and so on, are coupled. Figure 4 indicates that the tune shift is smaller for larger $|l|$. The threshold is higher when $|l|$ is larger. As shown in Fig. 14, the half-integer resonance for the $l = -2$ mode is the strongest.

The π modes are plotted using blue points. The tune shift is positive for the π mode. The tune of the $l = -2$ mode increases and crosses to $l = -3$ at $N^{(\pm)} = 0.7N_0$. No coupling occurs between the $l = -2$ (even) and $l = -3$ (odd) modes. The tune remains real even above $\geq 0.7N_0$. That is, instability only occurs at the σ mode for $\nu_x = 0.54$.

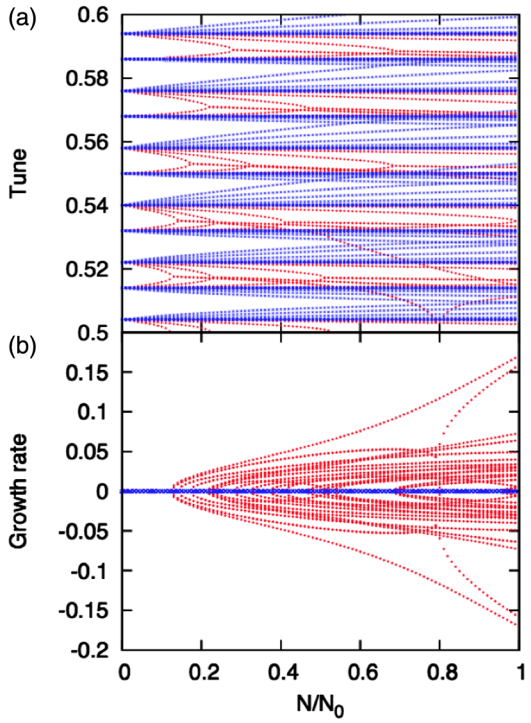

FIG. 14. Eigenvalues of σ and π modes as a function of the bunch population (N) for FCCee-Z parameter, where $\xi_x(N_0 = 10^{11}) = 0.025$, $\theta_P = 10$, $\nu_x = 0.54$, and $\nu_z = 0.018$. The tune and growth rate for scanning the bunch population $N^{(\pm)} = 0 - N_0$ are plotted in (a) and (b). Red and blue points are used for the σ and π modes, respectively.

Several lines start from the same tune with different radial modes, k. The threshold seems to be higher with the increase in k as the tune shift decreases with k.

The same calculation is carried out for $\nu_x = 0.55$. Figure 15 shows the variation in the (a) tune and (b) growth rate for the σ (red) and π (blue) modes. The tune of the $l = -3$ mode is closest to 0.5 but less than 0.5, $\nu_x - 3\nu_z = 0.496$. For increasing $N^{(\pm)}$, the tune shifts upward for the σ mode, Thus, it does not approach 0.5. The mode $\nu = 0.514(l = -2)$ reaches 0.5 at $0.4N_0$. For the instability of the σ mode, the threshold increases four times compared with that for $\nu_x = 0.54$. The modes with $l = -1, -3$ couple at a similar bunch population $0.4N_0$. The growth rates ($\mu_I = 0.22$) at N_0 are similar to that for $\nu_x = 0.54$.

The tune shift of the π mode is positive. For increasing $N^{(\pm)}$, the tune shifts downward for $l = -3$ (wrapped). Hence, it easily reaches 0.5 at $N^{(\pm)} = 0.2N_0$. The threshold decreases, while the growth rate above the threshold is lower compared with that of the σ mode. The π mode instability at $0.4N_0$ can be seen in the simulation of Fig. 9 (e). The growth rate of the σ mode is one order larger than that of the π mode at $N^{(\pm)} = N_0$, as seen in plot (b).

The same calculation is carried out for $\nu_x = 0.96$. The tune of the π mode increases at the reflected symmetric for

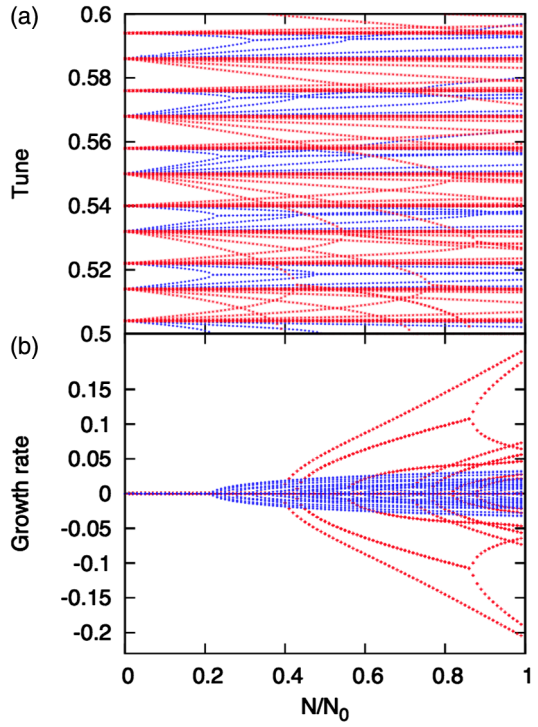

FIG. 15. Eigenvalues of the σ and π modes as a function of the bunch population for the FCC-ee-Z parameter, where $\nu_x = 0.55$ and $\nu_z = 0.018$. The tune and growth rate are plotted in (a) and (b), respectively. The red and blue points represent the σ and π modes, respectively.

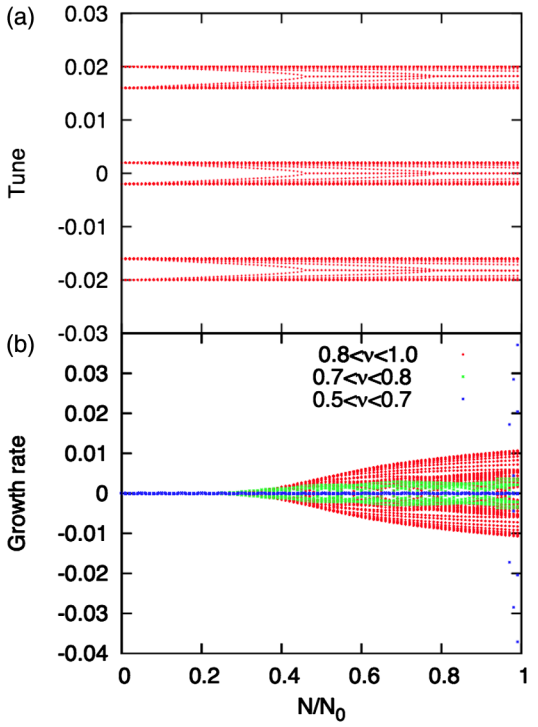

FIG. 16. Eigenvalues of the σ modes as a function of the bunch population for the FCC-ee-Z parameter, where $\nu_x = 0.75$ and $\nu_z = 0.018$. (a) Tune near $\nu = 0$ or 1. (b) Growth rate in the tune range $0.5 < \nu < 0.7$ (blue), $0.7 < \nu < 0.8$ (green), and $\nu > 0.8$ (red).

$\nu_x = 0.75$. The unstable π modes appear at the same $N^{(\pm)}$ as that for $\nu_x = 0.54$ and at the reflected tune for 0.75, that is, $1.5 - \nu$.

Figure 16 presents the (a) tunes and (b) growth rate of the σ modes at $\nu_x = 0.75$, where $n_k = 60$, $l_{\max} = 30$. It can be seen that beam instability arises and the beam shape is complex in the particle tracking in Fig. 9. It is seen that the higher-order mode is dominant for $\nu_x = 0.75$. It makes sense that the tune approaches from 0.75 to 0.5 at $l = 0.25/0.018 = 14$. Plot (a) shows the tune near $\nu = 0$ or 1. Mode-coupling behaviors are seen near $\nu = 0.5, 0.75$, and 1(0). Plot (b) shows the growth rate in the tune range $0.5 < \nu < 0.7$ (blue), $0.7 < \nu < 0.8$ (green), and $\nu > 0.8$ (red). The growth rate near $\nu \sim 0.5$ is the highest, that near $\nu \sim 1$ is medium, and that near $\nu \sim 0.75$ is low at N_0. A similar figure is obtained for the π mode; however, the order for the tune range of fast to slow growth is reversed.

These results enable the desirable tune for instability to be found. Choosing $\nu_x = (-n + 0.5)\nu_z$ (n is an integer) maximizes the distance between the σ and π modes. If the π mode is weak, it is possible to choose a somewhat higher tune.

We now consider the horizontal beam-beam tune shift discussed in Eqs. (10) and (11). When two Gaussian beams collide, each beam experiences a coherent tune shift of $\xi_x/2$. In Sec. II, the tune shift of the σ/π mode for the $k = l = 0$ mode was $\mp\xi_x/2$. The total tune shift of the σ mode is 0, whereas that of the π mode is ξ_x for the $k = l = 0$ mode. These tune shifts agree with the common understanding for the beam-beam tune shift. Considering the beam-beam tune shift, the synchro-betatron matrix M_0 in Eq. (37) can be replaced by

$$M_{0\xi} = e^{-2\pi i l \nu_z}\delta_{kk'}\delta_{ll'}\begin{pmatrix} 1 & 0 \\ -2\pi\xi_x & 1 \end{pmatrix}\begin{pmatrix} \cos\mu_x & \sin\mu_x \\ -\sin\mu_x & \cos\mu_x \end{pmatrix}. \tag{40}$$

Figure 17 presents the eigenvalues including the beam-beam tune shift as a function of the bunch population. All tunes of the σ and π modes shift in positive proportion to $N^{(\pm)}$. The threshold of the σ mode instability, which is $N^{(\pm)} = 0.2N_0$, increases twice, whereas the growth rate at N_0, $\mu_I = 0.15$, decreases slightly. These results agree with those of the particle-tracking results in Fig. 10. The π mode instability appears at $0.6N_0$, but the growth rate, $\mu_I = 0.03$, is 1/5 lower than that of the σ mode. Overall, these results do not qualitatively differ from the previous results without the beam-beam tune shift in terms of the appearance of the beam-beam instability.

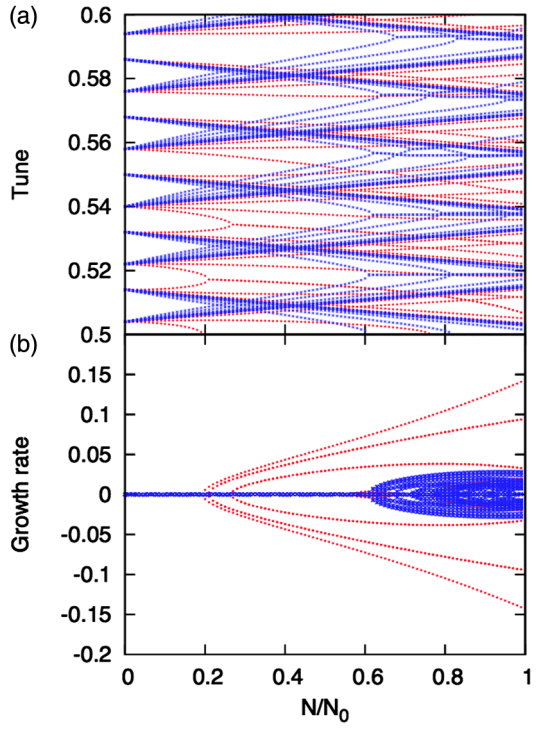

FIG. 17. Eigenvalues of the σ and π modes including the beam-beam tune shift ($\xi_x/2$) as a function of the bunch population (N) for FCCee-Z. The tune and growth rate for scanning the bunch population $N^{(\pm)} = 0 - N_0$ are plotted in (a) and (b), respectively. The red and blue points represent the σ and π modes, respectively.

V. EIGENVALUE PROBLEM FOR LOCALIZED CROSS-WAKE FORCE

A. Formalism for two-beam mode

The mode-coupling theory is extended to study two-beam modes correlated by the cross-wake force in Eq. (2). Two methods were used in the single-beam wake force: (1) dipole amplitudes discretized in longitudinal phase space and (2) expanded by azimuthal and radial modes. Both methods can be extended to the two-beam mode. We discuss an extension of the second method using the azimuthal (l) and radial (k) mode expansion. A vector for the dipole amplitudes of the $e^{\pm}$ beams is defined by $\boldsymbol{x}_{kl} = (x_{kl}^{(+)}, p_{kl}^{(+)}, x_{kl}^{(-)}, p_{kl}^{(-)})$. The length of the vector is $4 \times n_k(2l_{\max}+1)$. Each component is a coefficient of the kl expansion in Eq. (36). The vector is transferred by the matrices, M_s and M_β, for the synchrotron and betatron motion in a revolution, respectively. M_s is a diagonal matrix with the synchrotron phase advance, $e^{2\pi i l \nu_z}$,

$$M_s = \begin{pmatrix} e^{-2\pi i l \nu_s^{(+)}} & 0 \\ 0 & e^{-2\pi i l \nu_s^{(-)}} \end{pmatrix}, \tag{41}$$

where $\nu_z^{(\pm)}$ are the synchrotron tunes for the $e^{\pm}$ beam. Additionally, M_β consists of eight diagonal submatrices that describe the betatron motion with phase advances $2\pi\nu_x^{(\pm)}$ for the $e^{\pm}$ beams. The submatrices are diagonal, and their size is $[n_k(2l_{\max}+1)]^2$. The diagonal elements are $\sin\mu_x^{(\pm)}$ or $\cos\mu_x^{(\pm)}$,

$$M_\beta = \begin{pmatrix} \cos\mu_x^{(+)} & \sin\mu_x^{(+)} & 0 & 0 \\ -\sin\mu_x^{(+)} & \cos\mu_x^{(+)} & 0 & 0 \\ 0 & 0 & \cos\mu_x^{(-)} & \sin\mu_x^{(-)} \\ 0 & 0 & -\sin\mu_x^{(-)} & \cos\mu_x^{(-)} \end{pmatrix}. \tag{42}$$

The momentum change due to the cross-wake force is given by

$$\Delta p_{kl}^{(+)} = -2\sqrt{\beta_x^{(+)}\beta_x^{(-)}} \sum_{k'l'} M_{klk'l'}^{(+)} x_{k'l'}^{(-)}. \tag{43}$$

The matrix M is expressed by

$$M_{klk'l'}^{(+)} = \frac{1}{2} i^{l-l'-1} \int_{-\infty}^{\infty} d\omega Z_1^{(+)}(\omega) g_{kl}^{(+)}(\omega) g_{k'l'}^{(-)}(\omega), \tag{44}$$

where

$$g_{kl}^{(\pm)}(\omega) = \sqrt{\frac{1}{2\pi k!(|l|+k)!}} \left(\frac{\omega\sigma_{(\pm)}}{\sqrt{2}c}\right)^{2k+|\ell|} \exp\left(-\frac{\omega^2\sigma_{(\pm)}^2}{2c^2}\right), \tag{45}$$

where the impedance for the $e^{\pm}$ beam is provided in Eq. (17). The transfer matrix for $\boldsymbol{x}_{kl}$ is expressed by

$$M_W = \begin{pmatrix} 1 & 0 & 0 & 0 \\ 0 & 1 & -2M_{klk'l'}^{(+)} & 0 \\ 0 & 0 & 1 & 0 \\ -2M_{klk'l'}^{(-)} & 0 & 0 & 1 \end{pmatrix}. \tag{46}$$

The revolution matrix is represented by the product of the matrices $M_W M_s$ and M_β. They are symplectic matrices, and as such, the eigenvalues of the revolution matrix are expressed by $e^{\pm i\mu}$. The stability of the two-beam system is determined by μ.

B. Examples of two-beam mode

We discuss the two-beam mode for the three cases studied in the previous sections, (1) FCCee-Z, $\nu_x = 0.54/0.96$, (2) FCCee-Z, $\nu_x = 0.75$, (3) asymmetric collision of SuperKEKB, $\nu_x^{(+/-)} = 0.53/0.57$.

The eigensystem in two-beam formalism compares with that of the single beam in Sec. IV for FCCee-Z at $\nu_x = 0.54/0.96$, where $\xi_x = 0.025$, $\theta_c = 10$, and

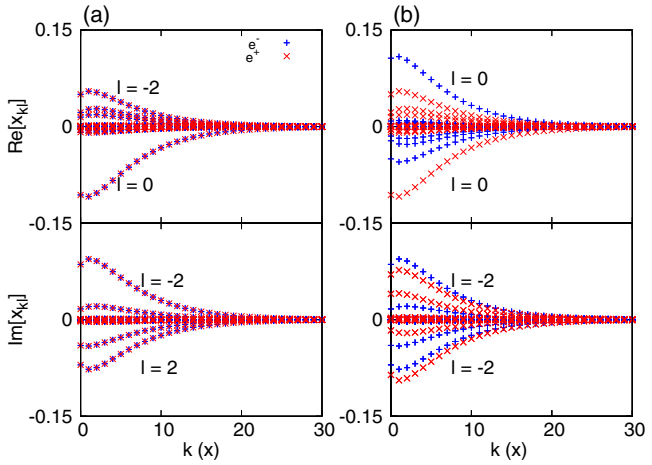

FIG. 18. Eigenvector $x_{kl}^{(\pm)}$ for the two-beam mode at the (a) horizontal tune $\nu_x = 0.54$ and (b) 0.96, as a function of k in FCCee-Z. The upper and lower plots are the real and imaginary parts of the eigenvector, respectively.

$\nu_z = 0.018$. The reliability of single-beam formalism assuming the σ or π mode is examined. The eigenvalue problem is solved for $n_k = 41, l_{\max} = 10$. The length of the vector $\boldsymbol{x}_{kl}$ is 3,444. The same plot as in Fig. 13 was obtained for the two-beam mode. The eigenvector informs the beam-beam mode with the eigentune. Figure 18 presents the eigenvector for the mode in which the eigenvalue has the largest absolute value. Plots (a) and (b) show $x_{kl}^{(\pm)}$ for the horizontal tune $\nu_x = 0.54$ and 0.96 as a function of k. The upper and lower plots are the real and imaginary parts of the eigenvector, x_{kl}, respectively. Several points with different l are plotted as a function of k. The eigenvector is significant for $k \leq 20$ $|l| \leq 7$, and $x(J, \phi)$ is reconstructed by the eigenvector x_{kl} using Eq. (36).

In plot (a), the eigenvector components are equal for the e^+ and e^- beams, $x_{kl}^{(+)} = x_{kl}^{(-)}$. A similar plot given for the momentum $p_{kl}^{(\pm)}$ indicates the same relation, $p_{kl}^{(+)} = p_{kl}^{(-)}$. Hence, the σ mode is excited at $\nu_x = 0.54$.

Conversely, in (b), the eigenvector components are opposite for the $e^\pm$ beams, $x_{kl}^{(+)} = -x_{kl}^{(-)}$. It can also be seen that $p_{kl}^{(+)} = -p_{kl}^{(-)}$. The π mode is excited at $\nu_x = 0.96$. The eigenvector for $\nu_x = 0.54$ or 0.96 in the two-beam mode explains the dominance of σ or π for $\nu_x <$ 0.75 or > 0.75 in Secs. III and IV.

In $\nu_x = 0.75$, eigenvalue analysis using a single beam exhibits instability for both the σ/π modes. This suggests that the assumption that either the σ or π mode arises for $\nu_x = 0.75$ is unsuitable. Therefore, the two-beam mode should be studied. Figure 19 presents the eigenvalues and growth rate as a function of the tune at N_0. Plots (a) and (b) show the eigenvalues for the two-beam and single-beam formalisms, respectively. In plot (b), the red and blue points represent the assumption of the σ and π modes, respectively. The growth rates for the tune in plots (a) agree with

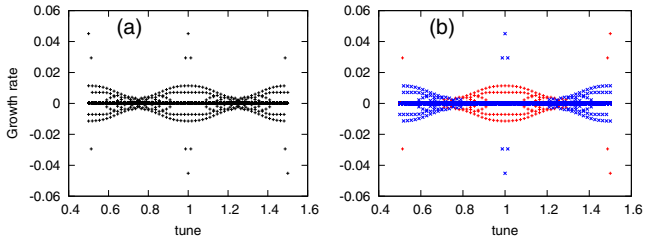

FIG. 19. Eigenvalues and growth rate as a function of the tune for the two-beam mode at $\nu_x = 0.75$ with the largest eigenvalue in the absolute, where $\xi_x = 0.025$ and $\theta_P = 10$ (FCCee-Z). (a) Two-beam mode and (b) single-beam mode with the assumption of a σ or π mode.

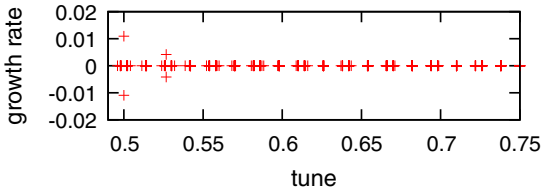

FIG. 20. Eigenvalues and growth rate as a function of the tune for $\nu_x^{(+)} = 0.53$ and $\nu_x^{(-)} = 0.57$ at SuperKEKB.

the merged rate of the σ and π modes in plot (b). The most unstable modes are $\nu = 0.5$ for the σ mode and $\nu = 1$ for the π mode. The eigenvectors corresponding to the modes were $x_{kl}^{(+)} = x_{kl}^{(-)}$ for $\nu = 0.5$ and $x_{kl}^{(+)} = -x_{kl}^{(-)}$ for $\nu = 1$. We found that single-beam formalism can be applied to the problem, even for $\nu_x = 0.75$.

When the transparency condition between the two beams is broken, it is clear that single-beam formalism cannot be applied. This is the only way to treat the two-beam mode. The particle-tracking results are presented in Fig. 11 for SuperKEKB, where the tunes of the $e^\pm$ beams are $\nu_x^{(+)} =$ 0.53 and $\nu_x^{(-)} = 0.57$, respectively. The beam parameters

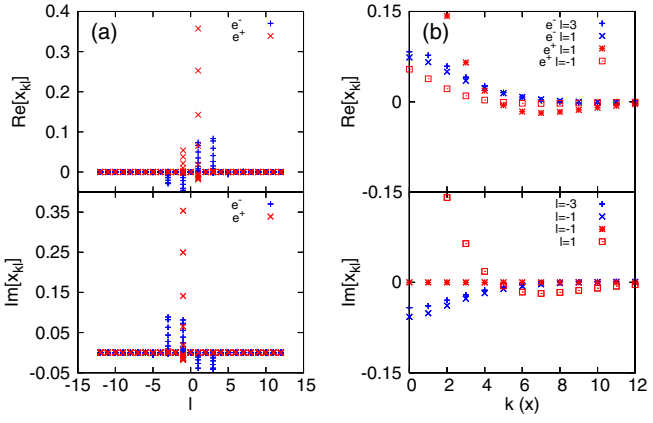

FIG. 21. Eigenvector of unstable mode with the fastest growth rate for $\nu_x^{(+)} = 0.53$ and $\nu_x^{(-)} = 0.57$ at SuperKEKB. (a),(b) Eigenvectors as functions of l and k, respectively.

are $\xi_x^{(+)} = 0.0174$, $\xi_x^{(-)} = 0.0099$, and $\theta_P = 8$. This suggests that the different azimuthal modes for the $e^{\pm}$ beams are excited. Figure 20 presents the eigenvalues and growth rate vs the tune for SuperKEKB. Unstable modes are seen at $\nu = 0.5$ and 0.528. Figure 21 presents an eigenvector with the largest eigenvalue in absolute terms. Plots (a) and (b) show the eigenvector as functions of l and k, respectively. The mode with the fastest growth is $l = \pm 1$ for the e^+ and $\pm 1, \pm 3$ for the e^- beam. This is reasonable when we recall the tune and the condition $\nu_x + l\nu_z \approx 0.5$.

VI. CONCLUSIONS

Beam-beam interactions with a large crossing angle induce a cross-wake force in which the dipole moment density of one beam provides a transverse kick to the other colliding beam. We obtained a formula for the cross-wake force, which could be treated as the usual single-beam wake force, assuming the same (σ mode) or opposite (π mode) dipole moment distributions of the two beams. The wake force did not exhibit instability in ordinary mode-coupling theory.

Particle-tracking simulations were examined using the single-beam wake and cross-wake force. σ mode instability was observed in the horizontal tune slightly above half an integer, $\nu_x = 0.54$. This tune is adopted in most lepton colliders to obtain high luminosity. For the single-beam wake force, assuming the existence of a π mode, instability did not occur. The simulations also showed that a localized wake force is essential to give rise to an instability.

Because the ordinary mode-coupling theory did not consider the localized wake force such as that induced by beam-beam interaction, a mode-coupling theory for the localized wake force was developed. Most of the characteristics of the instability seen in the tracking simulation are explained by the theory: the eigentune and number of unstable modes, the threshold of the instability, and the appearance of a σ or π mode.

The mode-coupling theory was further extended to treat the two-beam mode correlated by the cross-wake force without the assumption of the π or σ mode. We found the σ/π separation to be effective for two beams satisfying the transparency conditions on the beam-beam tune shifts and tunes. For asymmetric colliders such as SuperKEKB, it is essential to study the two-beam mode. Eigenvalues and eigenvectors for $\nu_x = 0.53/0.57$ for the $e^{\pm}$ beams were presented.

Future aspects that remain to be studied are the following. It is necessary to study the instability experimentally at SuperKEKB during the upcoming Phase-II commissioning. The strong-strong simulation showed the growth of the horizontal emittance above the instability threshold [3]. This growth appears to be caused by the damping of coherent motion and requires a detailed comparison with the strong-strong simulation. Other factors that require investigation are the effects of chromaticity, collisions with two interaction points, and combined phenomena coupled with beamstrahlung [25].

ACKNOWLEDGMENTS

The authors thank Dr. Y. Cai, Dr. D. Shatilov, Dr. Y. Zhang, and Dr. M. Benedikt for their fruitful discussions. This research project was supported, in part, by a Marie Skodowska-Curie RISE project of the European Commission's Horizon 2020 Programme under Contract No. 645479 E-Jade.

[1] A. Chao, *Physics of Collective Beam Instabilities in High Energy Accelerators* (Wiley-Interscience Publication, New York, 1993), and references therein.
[2] K. Ohmi, N. Kuroo, K. Oide, D. Zhou, and F. Zimmermann, Proceedings, 8th International Particle Accelerator Conference (IPAC 2017), Copenhagen, Denmark (2017), p. THPAB021.
[3] K. Ohmi, N. Kuroo, K. Oide, D. Zhou, and F. Zimmermann, Coherent Beam-Beam Instability in Collisions with a Large Crossing Angle, Phys. Rev. Lett. **119**, 134801 (2017).
[4] P. Raimondi, D. Shatilov, and M. Zobov, *Proceedings of 2nd SuperB Workshop, Frascati, 2006*.
[5] M. Zobov *et al.*, Test of "Crab-Waist" Collisions at the DAΦNE Φ Factory, Phys. Rev. Lett. **104**, 174801 (2010).
[6] D. Shatilov, E. Levichev, E. Simonov, and M. Zobov, Application of frequency map analysis to beam-beam effects study in crab waist collision scheme, Phys. Rev. ST Accel. Beams **14**, 014001 (2011).
[7] A. Bogomyagkov, E. Levichev, and D. Shatilov, Beam-beam effects investigation and parameters optimization for a circular e^+e^- collider at very high energies, Phys. Rev. ST Accel. Beams **17**, 041004 (2014).
[8] K. Ohmi and F. Zimmermann, *Proceedings, 5th International Particle Accelerator Conference (IPAC 2014): Dresden, Germany* (2014), p. THPRI004.
[9] K. Ohmi, *Proceedings, 7th International Particle Accelerator Conference (IPAC 2016): Busan, Korea* (2016).
[10] K. Ohmi, *Proceedings, 7th International Particle Accelerator Conference (IPAC 2016): Busan, Korea* (2016), p. MOZA01.
[11] See https://indico.cern.ch/event/615842/.
[12] See https://indico.cern.ch/event/617116/.
[13] K. Oide and K. Yokoya, Beam-beam collision scheme for storage-ring colliders, Phys. Rev. A **40**, 315 (1989).
[14] K. Hirata, Analysis of Beam-Beam Interactions with a Large Crossing Angle, Phys. Rev. Lett. **74**, 2228 (1995).
[15] M. Bassetti and G. Erskine, Report No. CERN ISR TH/80-06, 1980.
[16] F. Ruggieroand and F. Zimmermann, Luminosity optimization near the beam-beam limit by increasing bunch length or crossing angle, Phys. Rev. ST Accel. Beams **5**, 061001 (2002).
[17] D. Shatilov and M. Zobov, Beam-Beam Collisions with an Arbitrary Crossing Angle: Analytical tune shifts, tracking

algorithm without Lorentz boost, Crab-Crossing, ICFA Beam Dynamics Newsletter **37**, 99 (2005).
[18] A. Piwinski, DESY Report No. DESY 77/18, 1977.
[19] K. Oide *et al.*, Design of beam optics for the future circular collider e^+e^- collider rings, Phys. Rev. Accel. Beams **19**, 111005 (2016).
[20] H. Koiso, *Proceedings, 8th International Particle Accelerator Conference (IPAC 2017), Copenhagen, Denmark*, TUZB2 (2017), See http://www-superkekb.kek.jp/.
[21] Y. Funakoshi, *Proceedings of eeFACT16, 2016* (Cockcroft Institute, UK, 2016).
[22] F. Ruggiero, Transverse mode coupling instability due to localized structure, Part. Accel. **20**, 45 (1986).
[23] K. Oide, A mechanism of longitudinal single bunch instability in storage rings, Part. Accel. **51**, 43 (1995).
[24] A. J. Dragt, Lecture on nonlinear orbit dynamics, AIP Conf. Proc. **87**, 147 (1982).
[25] D. Shatilov (private communication).